Journal of Power Sources 200 (2012) 45–52

Contents lists available at SciVerse ScienceDirect

Journal of Power Sources

journal homepage: www.elsevier.com/locate/jpowsour

Manufacturing of anode-supported tubular solid oxide fuel cells by a new shaping technique using aqueous gel-casting

M.E. Navarro [a], X.G. Capdevila [a], M. Morales [a,*], J.J. Roa [b], M. Segarra [a]

[a] Centre DIOPMA, Departament de Ciència dels Materials i Enginyeria Metal·lúrgica, Universitat de Barcelona. C/Martí i Franqués 1, 08028 - Barcelona, Spain
[b] Laboratoire de Physique des Matériaux, Université de Poitiers, Bd Pierre et Marie Curie, BP 30179, 86962 - Futuroscope Chasseneuil Cedex, France

ARTICLE INFO

Article history:
Received 27 June 2011
Accepted 17 October 2011
Available online 21 October 2011

Keywords:
SOFC
Anode-supported tubular SOFC
Doped ceria
Manufacturing
Gel-casting
Extrusion

ABSTRACT

A new gel-casting technique has been successfully developed to obtain tubular NiO–SDC anode-supported solid oxide fuel cells (SOFCs). Rheological parameters of the ceramic particle suspensions, directly influencing on casting and production, were investigated as a function of process parameters: solid loading, dispersant and agarose amounts. Afterwards, a SDC ($Sm_{0.2}Ce_{0.8}O_{1.9}$) electrolyte film was deposited on NiO–SDC tubular anode substrates by colloidal spray-coating technique and co-sintering at 1400 °C for 5 h. The shrinkage and microstructure of the sintered cell components were studied. SEM results revealed high porosities of anode (40%) and cathode ($La_{0.5}Sr_{0.5}CoO_3$, LSC), a dense SDC film electrolyte with a thickness of 30 μm and a good adhesion between the electrolyte, and the anode and cathode.

1. Introduction

Solid oxide fuel cells (SOFCs) are electrochemical energy conversion devices with high efficiency and low emissions of pollution [1]. However, high temperature SOFCs based on yttria-stabilised zirconia (YSZ) requires the use of expensive materials and leads to significant problems with seals and interconnects. The development of intermediate temperature SOFCs (IT-SOFCs) reduces manufacturing costs, because it can be used cheaper metallic components as interconnectors and sealants.

Among alternative electrolyte materials, gadolinium-doped ceria (GDC) and samarium-doped ceria (SDC) are some of the most promising [2]. Both electrolytes present higher ionic conductivities than yttria-stabilised zirconia (YSZ) at intermediate temperatures (500–700 °C). However, GDC and SDC exhibit lower mechanical and redox stability than YSZ [3,4]. The partial reduction of Ce^{4+} to Ce^{3+} under reducing conditions leads to a significant n-type electronic conductivity, thus causing a partial internal electronic short-circuit in the cell [5,6]. In comparison with the traditional Ni–YSZ cermet anode, the Ni–SDC has various advantages derived from the extraordinary properties of the SDC compositions. SDC is an ionic and electronic mixed conductor under reducing atmospheres, which can increase the length of triple phase boundary (TPB) within the anode, thus enhancing the anode performance [7]. Moreover, SDC also exhibits a good catalytic activity for the oxidation of hydrocarbon fuels [8]. So, Ni–SDC presents low carbon deposition, and as a result, the catalyst deactivation is diminished [9,10]. Therefore, Ni–SDC cermet is considered as a interesting candidate for IT-SOFC anode operated under hydrogen and hydrocarbon fuels [11,12]. On the other hand, the electrochemical performance of cathodes, based on strontium cobaltite-based (LSC) perovskites, can be enhanced by adding doped ceria, which results in the suppression of growth of cobaltite particles. Therefore, the porosity can be maintained and the length of triple phase boundaries increased [13,14]. For this reason, the cathode will be composed by LSC and SDC (70–30 wt.%).

Related to its design, SOFC systems can be classified into: planar and tubular. Tubular stacks have some advantages such as higher mechanical and thermal stability, and simpler seal requirements, as they are only required where the manifolds connect to the cells. This area can be kept outside of the active cell zone where temperatures remain lower. For this reason, seals can overcome any change in load or fuel feed, which could yield to a temperature increase [15]. Moreover, as was reported by Kendall et al. [16] and Yashiro et al. [17], micro-tubular SOFCs could endure strong thermal stresses caused by rapid heating up to operating temperature. Use of small-scale tubular SOFCs allows to design cell stacks with high volumetric power density as the electrolyte area per volume unit increases [18]. On the other hand, the ionic conductivity of an anode-supported fuel cell with a thin-film electrolyte at low temperature is higher than that of an electrolyte-supported one, due to the decrease of electrolyte resistance losses [19,20].

* Corresponding author. Tel.: +34 934034711; fax: +34 934035438.
E-mail address: mmoralescomas@yahoo.es (M. Morales).

0378-7753/$ – see front matter © 2011 Elsevier B.V. All rights reserved.
doi:10.1016/j.jpowsour.2011.10.059

Manufacturing is one of the major focuses of SOFC cost reduction. Among manufacturing techniques, gel-casting is a well-established colloidal processing method with a short forming time, high yields and low-cost equipment [21]. It can be used to prepare high-quality and complex-shaped from dense to porous ceramic modules. During gel-casting, the macromolecular gel network results from the *in situ* polymerisation of organic monomers added to the suspensions, holding the ceramic particles together. Then gel achieves enough strength to support its own weight and it can be handled without shape distortion [22]. Finally, this method can be used to shape the anode-supported tubular fuel cell both in laboratory and at industry scale [23,24].

In the present work, the aqueous gel-casting process has been successfully developed to obtain tubular NiO/SDC anode-supported SOFCs. The synthesis of the raw materials was performed by the polyacrylamide gel combustion method. Rheological behaviour of the ceramic particle suspension for gel-casting was investigated as a function of the process parameters. Afterwards, tubular anode was shaped by a new forming technique, which operates as a syringe. Thin-film SDC as an electrolyte was deposited by spraying method. Both anode and electrolyte were co-sintered at an optimized temperature and time from the obtained results of a design of experiments (DoE). The main objective of this method is to increase the productivity of the experimental process by lowering the number of experiments and increasing the accuracy of the results. It has been used in fuel cells field to optimize materials and components [25,26], and also to analyze and evaluate the performance of single cells and stacks [27]. As previously reported [28], we used the DoE method to optimize the anode microstructure of the fuel cell. After that, LSC–SDC (70–30 wt.%) as a cathode was deposited by spraying and sintered. Finally, microstructures of selected tubes were evaluated by SEM.

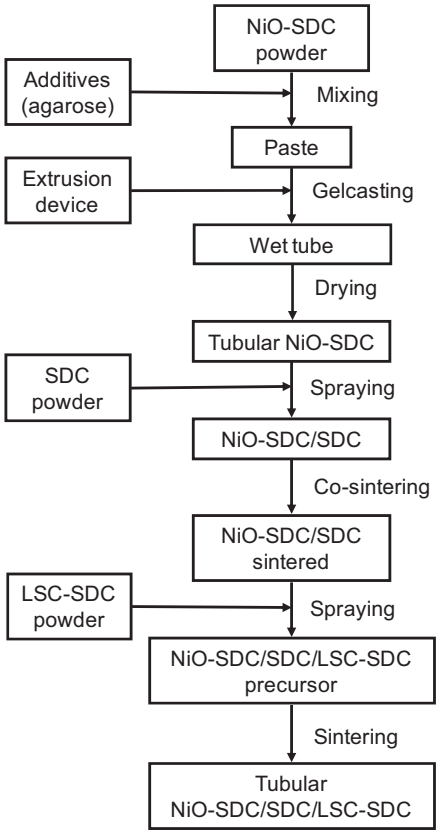

Fig. 1. Diagram of the process to obtain NiO–SDC tubes.

2. Materials and experimental procedure

Samarium-doped ceria, nickel oxide-samarium doped ceria (60:40 wt.%) and lanthanum strontium cobaltite powders, with a nominal composition of $Sm_{0.2}Ce_{0.8}O_{1.9}$, NiO–$Sm_{0.2}Ce_{0.8}O_{1.9}$ (NiO–SDC) and $La_{0.6}Sr_{0.4}CoO_3$ (LSC) respectively, were synthesized by polyacrylamide gel combustion as described elsewhere [29]. The materials were prepared from Sm_2O_3 (Strem Chemical 99.9%), CeO_2 (Strem Chemical 99.9%), La_2O_3 (Alfa Aesar 99.9%), $Sr(CH_3COO)_2$ (Pro-BVS 99%), $Ni(CH_3COO)_2$ (Alfa Aesar 99%) and $Co(CH_3COO)_2$ (PANREAC 99%). After combustion, the materials were calcined at 500 °C for 2 h to assure the total organic removal [29]. All these powders were characterized by BET specific surface and XRD. Morphological analysis of the powders was performed by scanning electron microscopy (SEM) and transmission electron microscopy (TEM).

Afterwards, porous anode tubes were prepared by aqueous gel-casting technique. The experimental procedure used to shape NiO–SDC tubes is shown in Fig. 1. Ceramic suspensions with anode powder and distilled water were prepared by adding a commercial dispersant (DOLAPIX Zschimmer & Schwarz Spain, S.A.) Homogenization was performed by an ultrasonic finger (Sonics Vibracell VCX-130). Agarose solution was prepared by adding an industrial agar (Conda Lab.) and then activated by heating above 80 °C. The agarose solution must be maintained above a determined temperature until casting in order to avoid a premature gelation. To determine the gelation temperature of the paste, the system viscosity was studied with the temperature using a viscosimeter (HAAKE Viscotester 6R plus). In this step, the optimization of several process parameters such as solid loading (20–30 wt.%), dispersant concentration (0.2–3 wt.%) and agarose amount (0.25–2 wt.%) were investigated. The tubes were extruded from the gel-casting using a punch (∅ = 6 mm) with an in-house-designed die (∅ = 10 mm).

After drying the tubes in air, they were cut to length. Previously to the colloidal spraying deposition of the electrolyte, SDC powder was ball-milled in ethanol media for 6 h using a zirconia jar and yttria balls (5 mm diameter) to decrease and homogenize the particle diameter. A rotational speed of 300 rpm was used during ball milling. The colloidal suspension for spray-coating was made by mixing the corresponding powder with terpineol (1:2 wt.%). The final suspension was ultrasonically mixed. An air pressure-assisted spray was used to deposit the SDC colloidal suspension onto the rotating tubular anode substrate. The spray conditions such as nozzle distance, the rotational speed of substrate, nozzle speed, and air pressure were studied. After that, the film electrolyte of the tubular half-cell was dried in air. The tubes were vertically hung on a sample holder to remain straight during sintering.

Finally, both anode and electrolyte were co-sintered. In order to optimize the anode porosity at different process parameters, DoE was performed by using factorial experiments instead of the classical one-factor-at-a-time method. It allowed to determine the interactions between the studied parameters. A type of response surface design known as Box-Behnken design was used (Fig. 2). It allows to exclude the cube corners, because all variables are simultaneously determined at the maximum levels. This experiment matrix consisted of three factors with three levels for each one. So, the slope rate of heating (2, 5 and 10 °C min^{-1}), temperature (1300, 1350 and 1400 °C), and time (2, 3.5 and 5 h) were studied. The DoE results were analyzed by Statgraphics Plus Software. The total (open and close) anode porosity was then determined from the difference between the theoretical and real density, and using a helium gas absorption pycnometer (Micromeritics) to determine the apparent density.

After co-sintering treatment, the anode tubes with electrolyte were spray-coated with a LSC–SDC (70–30 wt.%) cathode suspension. Cathode powders were firstly ring-milled for 60 s in a WC ring

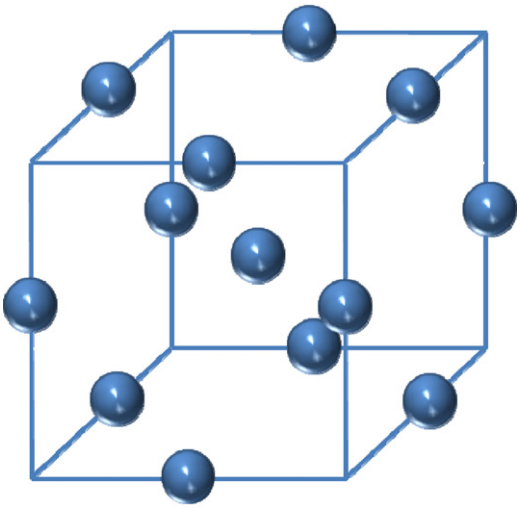

Fig. 2. Graphical representation of the Box-Behnken Design.

mill. The LSC precursor was also mixed with terpineol (1:2 wt.%) to make the colloidal suspension and sprayed onto the SDC electrolyte of NiO–SDC/SDC tube. After spray-coating the cathode slurry, the tubes were dried in air and sintered at temperatures of 800–900 °C in air for 2 h to complete the cell. Finally, the fuel cell microstructure was examined by electron microscopy (SEM).

3. Results and discussion

3.1. Characterization of powders

The XRD patterns of NiO–SDC and SDC powders presented no evidences of secondary phases. An anode specific surface of 40 $m^2 g^{-1}$ and a particle size of 20 nm were obtained by BET technique. Morphological analysis of the powders was performed by Hitachi H-2300 scanning electron microscopy (SEM) and is shown in Fig. 3a and b. A spongy morphology of NiO–SDC and SDC powders was observed, which was attributed to the gases generation during combustion process. Homogeneous powders without segregation and agglomerates were obtained after combustion process. So, the synthesis by polyacrylamide gel combustion allows to obtain nanometric powders with high surface area. A good dispersion between both phases was achieved. Additionally, morphological analysis of the SDC powders, using a Philips 301 transmission electron microscopy (TEM), is presented in Fig. 3c. A good homogeneous distribution of faceted grains with a grain size smaller than 50 nm is observed, which is according to the BET results.

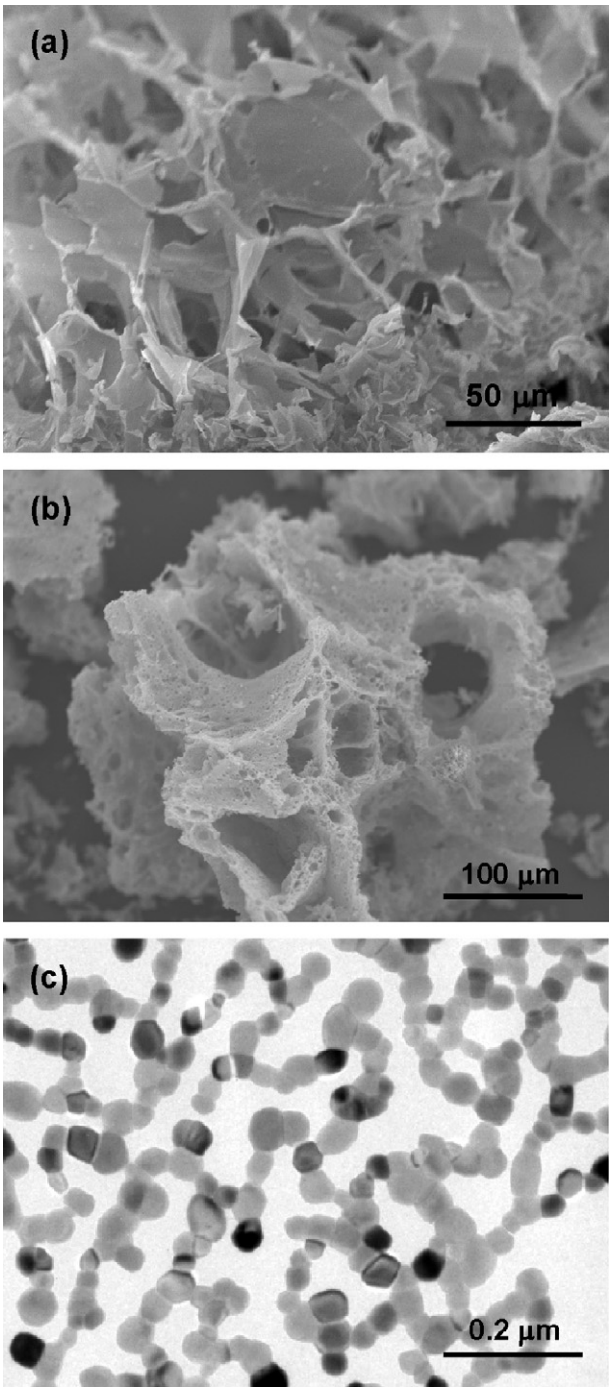

Fig. 3. SEM images of NiO–SDC (a) and SDC (b); and TEM image of SDC (c).

3.2. Formulation and preparation of paste

The properties of NiO–SDC anode microstructure depends on the distribution of NiO, SDC and porosity, which is strongly affected by the rheological behaviour of suspension. Lower viscosity helps to increase the dispersion of particles, suspension homogeneity, degassing, casting, and lack of defects. Many authors have found that several factors affect the rheological behaviour of suspension, such as pH value, dispersant, monomer, and/or solid loading [24,30]. However, all these factors differ from one system to another. So, this study will involve the following parameters: solid loading, dispersant concentration and agarose amount.

A higher solid loading in the suspension leads to a higher suspension viscosity and density of the final ceramic. However, the SOFC anodes should be porous, and therefore, a high solid loading is not required. Solid loading also affects the sintering shrinkage rate [31]. So, it must be considered for the co-sintering process with anode-electrolyte. Generally, the required shrinkage of the anode-support should be equal to or slightly higher than that of the electrolyte layer to obtain a dense one [24]. The preliminary results indicated that a suitable suspension of solid loading was between 20 and 30 wt.%. Later, this experimental parameter will be settled depending on the other variables. Other researchers such as Dong et al. [24] and Bao et al. [32] found that the shrinkage rate of sintered NiO–YSZ and YSZ at 1400 °C for 5 h were 21.6% (with a solid loading of 45%) and 20.5%, respectively.

The dispersant concentration can prevent the particles aggregation by absorbing on the particles surface and enhances the green body strength made by gel-casting. The amount of dispersant

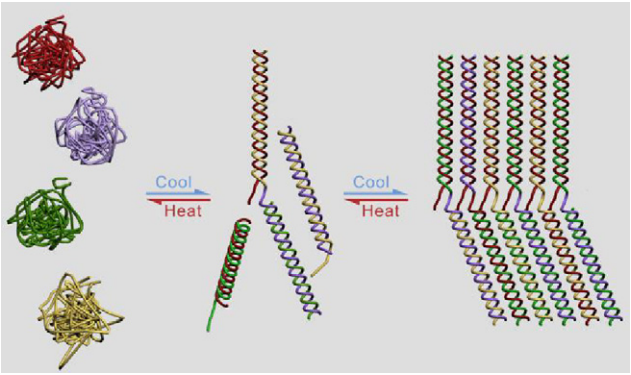

Fig. 4. Cross-linking process.

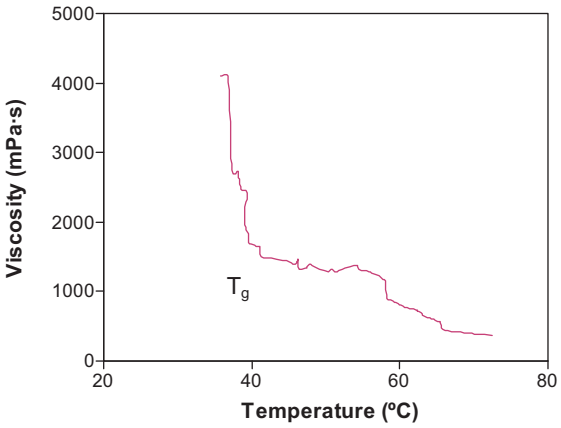

Fig. 5. Evolution of viscosity as a function of temperature of aqueous solution with 1 wt.% agar.

added to different suspensions of anode powder in distilled water (20–30 wt.%) was studied within the concentration range from 0.2 to 3 wt.% vs. powder. When the dispersant concentration was higher than 2 wt.%, its efficiency was decreased and the oxide particles were coarsened again. So, ceramic suspensions with anode powder and distilled water were prepared by adding 1 wt.% commercial dispersant vs. powder. After that, the suspensions were homogenized by an ultrasonic finger.

Agarose was used as a gelling agent. This cross-linker produces a network of helicoidal chains, thus resulting structures with double helix (Fig. 4). The immobilization and consolidation of particles occurs under cooling conditions, below glass transition temperature (T_g). When the agarose gel is heated again, it can be redissolved [33]. It is possible to optimize the agarose amount in the final gel in order to obtain a stiff structure, which keeps its form after shaping. The extrusion of tubular cells from agarose gel-casting, at temperatures slightly higher than room ones and atmospheric pressure, leads to a simple and scalable method for industrial production of tubular cells. So, it is an interesting method to shape tubular cells, being also non-pollutant and biodegradable. The suspension viscosity is significantly affected by the agarose amount. Like the dispersant, the agarose plays an important role for the steric stabilization and the viscosity. So, the agarose concentration to achieve a suitable casting was determined by the suspension viscosity and the strength of the cast green body. For low concentrations of agarose (<0.75 wt.%), the casting bodies were deformed by its own weight. When the agarose content was higher than 1.5 wt.%, the high viscosity was not suitable for casting, thus becoming difficult to fill up the mould. It was found that around 1 wt.% vs. water (for 20–30 wt.% powder/water) is the minimum agarose amount to obtain a suitable green tube, strong enough to avoid its plastic deformation during handling. The viscosity of the 1% agarose suspension was studied as a function of temperature in order to evaluate the stability of the agarose at the suitable temperature. At temperatures higher than 85 °C, the agarose suspension is activated. On cooling, the gelation occurs at T_g around 40 °C (Fig. 5). Similar results were reported by A. J. Millan et al. [33]. So, the suspension must be maintained above 39 °C until casting to avoid a premature gelation.

3.3. Tube gel-casting

For the proposed process, the tubes were shaped from the anode slurry using a home-made device. Fig. 6 shows a schematic view of the equipment, which has two different sections: the reservoir and the syringe. The reservoir, which contains the slurry, is closed and made of silicone to prevent temperature gradients and slurry gelation. The reservoir is conical to allow a free flow of the slurry towards the syringe, which is a simple piston pump consisting of a plunger that fits tightly in a glass tube as a die. A steel punch is concentrically placed inside the die to obtain the hollow section of the tubes. The plunger can be handly moved, pulling or pushing along the tube, thus allowing to take in, gelify and expel the body through the end of the tube. The die length depends on the production rate and the dimensions of the final tubular cell. Wet anode tubes up to 40 cm were successfully obtained with this methodology.

As a plastic forming method, minimum mechanical requirements are necessary. The paste should be plastic enough to shape the body into desired form under the applied load. A good strength in wet conditions is also needed. After the material is shaped, the green body must be strength enough to avoid the tube deformation due to its own weight and the handling stresses. Therefore, careful handling is required when the green body is expelled. Finally, the resulting green tubes are dried in air for 24 h. As shown in Fig. 7a, we are usually shaping 25 cm length tubular anode-supported fuel cells with this forming method. It is possible to obtain a wide diameter range of tube combining different diameters of die and punch (Fig. 7b and c). Geometrical parameters of different anode substrates, after drying in air and sintering at 1400 °C for 5 h, are listed in Table 1.

3.4. Spray-coating and co-sintering of the anode/electrolyte

The electrolyte quality strongly affects the final cell performance. So, it should be dense enough to achieve a gas tight layer

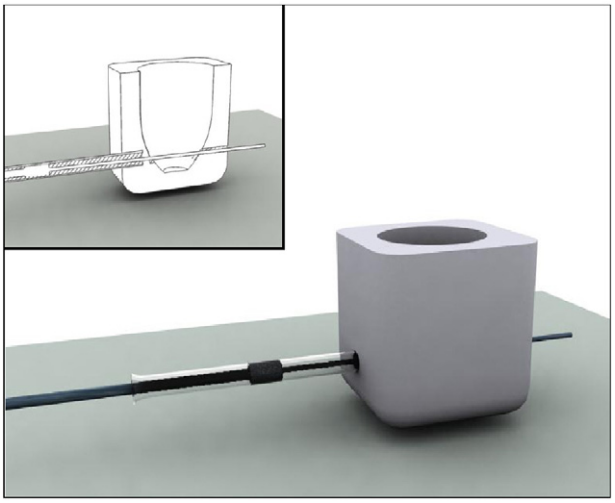

Fig. 6. Schematics of the extrusion device.

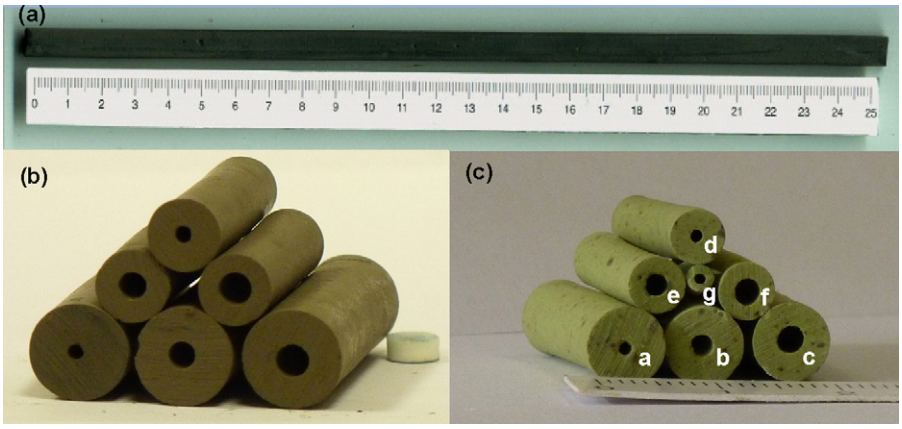

Fig. 7. 25 cm length tubular anode (a). Green (b) and sintered (c) tubes with several inner and outer dimensions. (For interpretation of the references to color in this figure legend, the reader is referred to the web version of the article.)

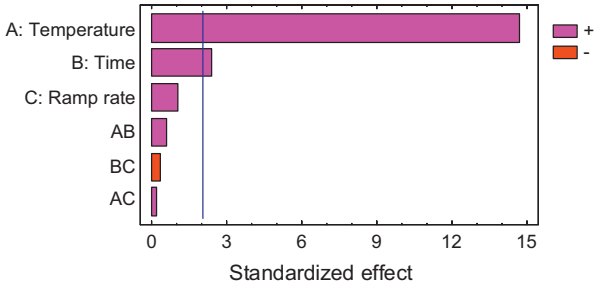

Fig. 8. Standardized Pareto effect for anode density on the sintering parameters.

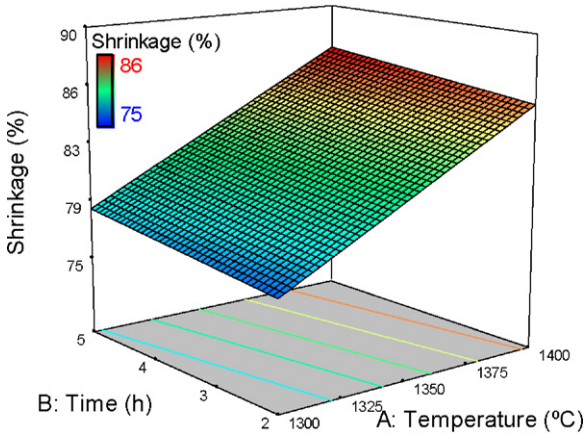

Fig. 9. Response surface for shrinkage as a function of co-sintering temperature and time.

and thin enough to reduce the ohmic resistance. Uniform, pinhole-free and microcrack-free films can be obtained by spray-coating method. In the present work, multiple thin layers were deposited without defects.

Analysis of the design of experiments was performed, for the co-sintering process, on the basis of the analysis of variance, a collection of models in which the observed variance is partitioned into components (heating rate, sintering temperature and time) due to different factors, which are estimated and/or tested. Fig. 8 shows the standardized Pareto Chart for the anode density response. The different effects of each factor on the density were represented by bars. They were sorted in descending order from the most significant factor to the least one. The length of each bar is proportional to the standardized effect, which equals to the t-statistic magnitude that would be used to test the statistical significance of that effect. Some bars, which extend to the right line, indicate that the factor effects are statistically significant at the 5% significance level. So, these results indicated that the density was not significantly influenced by the heating rate within the range from 5 to 10 °C min^{-1}. In contrast, it was found that the density was positively affected by both sintering temperature and time. When the temperature and time were increased, the anode density also increased, while porosity decreased. However, the effect of the sintering temperature on the density was much higher than that of the sintering time.

In Fig. 9, the tube shrinkage as a function of co-sintering temperature and time is presented. Sintering effect starts above 1000 °C. Mechanical properties and reduction ratios up to 75% are obtained between 1000 and 1400 °C. In addition, Fig. 10 shows the correlation between the porosity of the anode tubes and the co-sintering temperature and time. The tube porosity decreased as the co-sintering temperature approached 1400 °C, which was significantly reduced to ~40%. Finally, an outstanding anode porosity and dense electrolyte film were successfully obtained by a co-sintering process at 1400 °C for 5 h. It will be sustained in further electrical measurements.

Table 1
Geometrical parameters of the tubular anode before and after sintering at 1400 °C.

Sample	Mould		After drying			After sintering		
	$\varnothing_{outer}$ (mm)	$\varnothing_{inner}$ (mm)	$\varnothing_{outer}$ (mm)	$\varnothing_{inner}$ (mm)	Length (mm)	$\varnothing_{outer}$ (mm)	$\varnothing_{inner}$ (mm)	Length (mm)
a	10	2	9.5	1.5	33.0	6.4	1.2	22.9
b	10	3	9.5	2.6	32.5	6.6	1.9	22.3
c	10	4	9.5	3.2	35.0	6.7	2.2	23.9
d	10	6	9.5	4.5	31.7	6.8	3.1	21.2
e	7	2	6.7	1.5	31.0	4.6	1.0	20.9
f	7	3	6.7	2.5	30.0	4.8	1.8	19.7
g	7	4	6.7	3.3	27.5	4.8	2.3	18.3
h	5	2	4.2	1.5	16.5	2.4	1.0	9.1

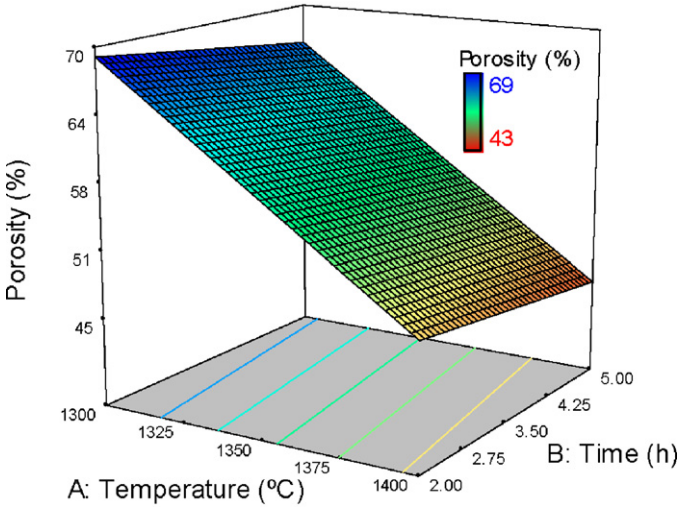

Fig. 10. Porosity of the NiO–SDC anode tubes as a function of the co-sintering temperature and time.

In Fig. 11, we can observe the obtained NiO–SDC/SDC tube after electrolyte spraying and co-sintering. The inner and outer diameters after co-sintering were 2.5 mm and 5 mm, respectively, thus resulting in an overall volume reduction of 85%.

3.5. Spray-coating and sintering of the cathode

After co-sintering treatment, the anode tubes with electrolyte were spray-coated with the cathode suspension, dried in air for 24 h, and sintered at temperatures of 800–900 °C in air for 2 h to complete the cell. So, the LSC powders were crystallized to the perovskite phase and simultaneously sintered with SDC powders. This method in only one step provides several advantages: (i) the reduction of the preparation cost of cathode, because the sintering of LSC powders before spray-coating is avoided; (ii) the composition of electrode materials can be controlled and (iii) the adhesion between the electrode and electrolyte is outstanding, due to the submicrometric size of powders. However, it is possible that secondary and/or insulating phases can be formed. So, the effect of sintering temperature on crystallization of the LSC perovskite has been investigated by XRD. Patterns of XRD as-prepared and at different sintering temperatures of LSC powders are presented in Fig. 12. The as-prepared LSC powders were slightly crystalline. At

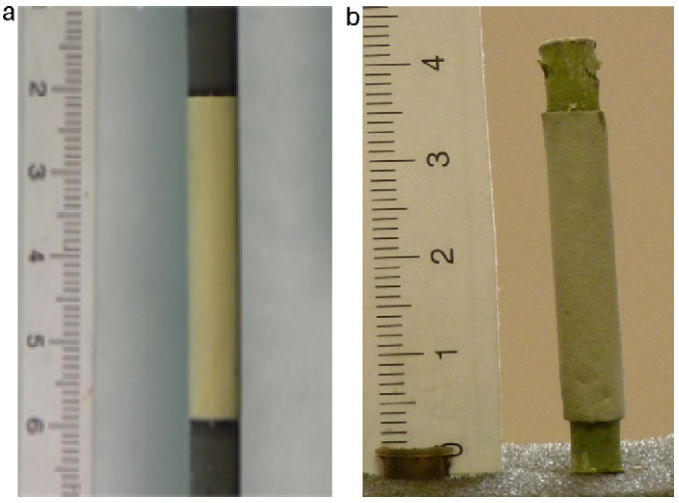

Fig. 11. Image of NiO–SDC/SDC tube before (a) and after (b) co-sintering.

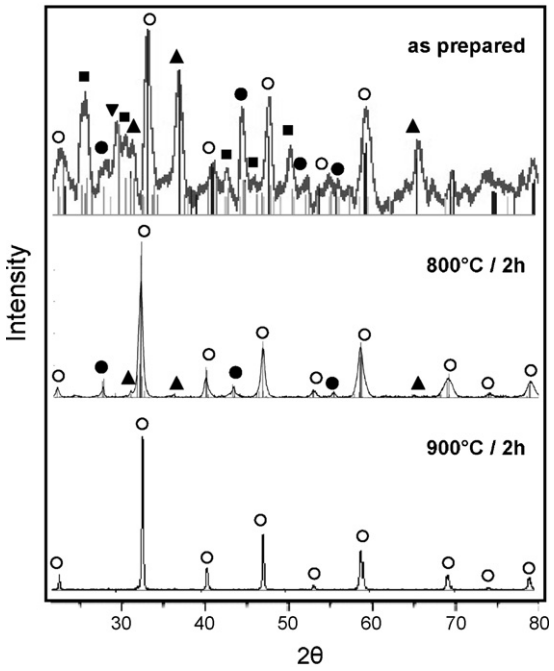

Fig. 12. XRD patterns corresponding to the as-prepared and at different sintering temperatures of LSC powders. Phases: $La_{0.5}Sr_{0.5}Co_{3-\delta}$ (○), $SrCoO_{2.52}$ (●), Co_3O_4 (▲), $La_2O_2CO_3$ (▼), and $SrCO_3$ (■).

800 °C, some secondary phases were appeared, which mean that the crystallization to the perovskite phase was not completely formed at this temperature. At 900 °C, it is found that pure, well-crystallized LSC was formed.

3.6. Microstructural characterization

The final size of single cell was 5 mm of outer diameter (2.5 mm of inner diameter) and 8 cm length with an active cathode length of 6 cm, which resulted in an active area of 12.5 cm^2. Cross-sectional scanning electron microscopy (SEM) images of the anode tube with electrolyte after co-sintering at 1400 °C for 5 h are presented in Fig. 13. The anode is the inner layer, where the fuel flows through the single-cell tube. The outer layer is the cathode, where air flows around. As can be seen in Fig. 13c, a dense electrolyte, without pinholes and crack-free, with a thickness of about 30 μm was successfully prepared on the tubular anode by co-sintering technique. A relatively outstanding anode interconnected porosity and a good adhesion between the anode and the electrolyte were also observed. The anode microstructure by BSE-SEM is presented in Fig. 13d. NiO particles can only be roughly distinguished according to their slightly lower brightness than SDC grains. Although nano-sized NiO and SDC particles were used as the starting material, they were grown during the co-sintering process. However, a highly homogeneous and porous anode without agglomeration of NiO nor SDC particles was obtained. Both facts will probably lead to a high catalytic active area. The electrolyte-cathode interface and cathode microstructure are shown in Fig. 13e and f. LSC–SDC cathode of 30 μm thickness presents a good adhesion to the electrolyte. It is also observed that the cathode exhibits a highly porous and thin microstructure. It will probably have a significantly effect on the electrode performance, as the presence of pores facilitates the gas transfer, thus increasing the number of active reaction sites.

Future work will be focused on the electrical characterization of the tubular cells obtained by gel-casting technique as well as the influence of anode thickness on the mechanical properties and the electrical performance. Then the effect of anode thickness on

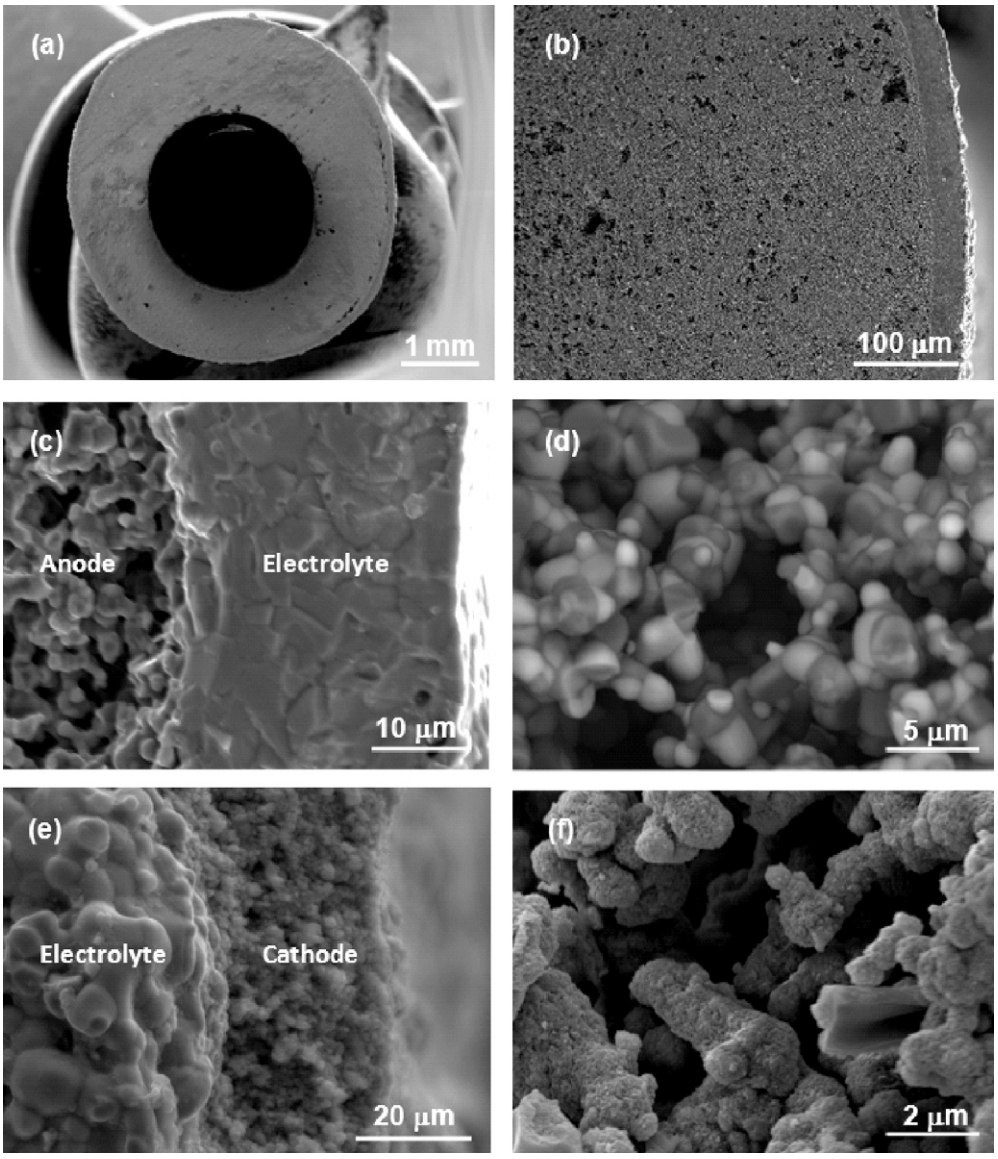

Fig. 13. Cross-sectional SEM micrographs of: (a) and (b) the tube after co-sintering at 1400 °C for 2 h in air, (c) anode-electrolyte interface, (d) anode microstructure, (e) electrolyte–cathode interface, and (f) cathode microstructure.

the mechanical resistance and mass transport losses, etc. will be investigated. It will be the subject of a future publication.

4. Conclusions

In this work, a cost-effective gel-casting technique was successfully developed to obtain anode-supported tubular SOFCs. Rheological parameters of the ceramic particle suspensions, directly influencing on casting and production, were investigated. A suitable relation between slurry viscosity, porosity and mechanical strength of tubes was found. Under these conditions, an agarose suspension prepared by mixing 1 wt.% agarose vs. water above 80 °C was attained, which was suitable for gel-casting. For the proposed gel-extrusion process, the tubes were shaped from the gel-casting using a new and simple forming technique, which was based on a syringe, using a punch with an in-house-designed die. The real cost of the process has not widely studied. Although only comparing the cost of the reagents and equipment gives an idea of the savings. Then, a SDC electrolyte film was successfully deposited on NiO–SDC tubular anode substrates by colloidal spray-coating technique and co-sintering at 1400 °C for 5 h. After that, $La_{0.5}Sr_{0.5}CoO_3$ (LSC) as a cathode was deposited by a spraying method and sintered at 900 °C for 2 h in air. SEM results revealed high porosities of anode (40%) and cathode, a dense SDC film electrolyte with a thickness of 30 μm, and a good adhesion between the electrolyte and electrodes. Electrical characterization of the tubular single cell will be further performed.

Acknowledgements

This work has been partially supported by the Ministerio de Ciencia e Innovación under project MAT2008-06785-C02-01 and the Xarxa de Referència en Materials Avançats per l'Energia (XaRMAE, Generalitat de Catalunya). The authors would like to thank Zschimmer & Schwarz Spain, S.A and Laboratorios Conda for their materials supply.

References

[1] Fuel Cell Handbook, Seventh ed., EG&G Technical Services, Inc., University Press of the Pacific, 2004.

[2] J. Fergus, R. Hui, X. Li, D.P. Wilkinson, J. Zhang, Solid Oxide Fuel Cells: Materials Properties and Performance, CRC, 2008.
[3] M. Morales, J.J. Roa, X.G. Capdevila, M. Segarra, S. Piñol, Acta Mater. 58 (7) (2010) 2504–2509.
[4] S. Piñol, M. Morales, F. Espiell, J. Power Sources 169 (2007) 2–8.
[5] V.V. Kharton, F.M.B. Marques, A. Atkinson, Solid Oxide Ionics 174 (2004) 135–149.
[6] D. Hirabayashi, A. Tomita, S. Teranishi, T. Hibino, M. Sano, Solid State Ionics 176 (2005) 881–887.
[7] C.W. Sun, U. Stimming, J. Power Sources 171 (2007) 247–260.
[8] S. Zhao, R.J. Gorte, Appl. Catal. A 277 (2004) 126–129.
[9] M. Yano, A. Tomita, M. Sano, T. Hibino, Solid State Ionics 177 (2007) 3351–3359.
[10] T. Ida, M. Kawano, T. Matsui, R. Kikuchi, K. Eguchi, J. Electrochem. Soc. 154 (2007) B234–B241.
[11] E. Perry Murray, T. Tsai, S.A. Barnett, Nature 400 (1999) 651–659.
[12] M. Morales, S. Piñol, M. Segarra, J. Power Sources 194 (2009) 961–966.
[13] C. Xia, W. Rauch, F. Chen, M. Liu, Solid State Ionics 149 (2002) 11–19.
[14] J. Zhang, Y. Ji, H. Gao, T. He, J. Liu, J. Alloys Compd. 395 (2005) 322–325.
[15] C.E. Hatchwell, N.M. Sammes, K. Kendall, J. Power Sources 70 (1998) 85.
[16] K. Kendall, M. Palin, J. Power Sources 71 (1998) 268–270.
[17] K. Yashiro, N. Yamada, T. Kawada, J. Hong, A. Kaimai, Y. Nigara, J. Mizuski, Electrochemistry 70 (12) (2002) 958–960.
[18] Y. Funahashi, T. Shimamori, T. Suzuki, Y. Fujishiro, M. Awano, J. Power Sources 163 (2) (2007) 731–736.
[19] Z. Shao, C. Kwak, S.M. Haile, Solid State Ionics 175 (2004) 39–46.
[20] M. Morales, J.J. Roa, X.G. Capdevila, M. Segarra, S. Piñol, Fuel Cells 11 (1) (2011) 108–115.
[21] A.J. Millán, I. Santacruz, A.J. Sánchez-Herencia, M.I. Nieto, R. Moreno, Adv. Eng. Mater. 4 (12) (2002) 913–915.
[22] J. Yang, J. Yu, Y. Huang, J. Eur. Ceram. Soc. 31 (14) (2011) 2569–2591.
[23] O.O. Omatete, M.A. Janney, S.D. Nunn, J. Eur. Ceram. Soc. 17 (1997) 407–413.
[24] D. Dong, J. Gao, X. Liu, G. Meng, J. Power Sources 165 (2007) 217–223.
[25] M.G. Medeiros, R.R. Bessette, C.M. Deschenes, D.W. Atwater, J. Power Sources 96 (2001) 236–239.
[26] R. Küngasa, I. Kivia, K. Lusta, G. Nurka, E. Lust, J. Electroanal. Chem. 629 (1–2) (2009) 94–101.
[27] B. Wahdamea, D. Candussob, X. Françoisa, F. Harelb, J.M. Kauffmanna, G. Coqueryb, Int. J. Hydrogen Energy 34 (2) (2009) 967–980.
[28] A. Faes, J.M. Fuerbringer, D. Mohamedi, A. Hessler-Wyser, G. Caboche, J. Van Herle, J. Power Sources 196 (2011) 7058–7069.
[29] A. Douy, Int. J. Inorg. Mater. 3 (7) (2001) 699–707.
[30] X. Liu, Y. Huang, J. Yang, Ceram. Int. 28 (2002) 159–164.
[31] K. Niihara, B.-S. Kim, T. Nakayama, T. Kusunose, T. Nomoto, A. Hikasa, T. Sekino, J. Eur. Ceram. Soc. 24 (2004) 3419–3425.
[32] W. Bao, Q. Chang, G. Meng, J. Membr. Sci. 259 (2005) 103–109.
[33] A.J. Millán, R. Moreno, M.I. Nieto, J. Eur. Ceram. Soc. 22 (2002) 2209–2215.